Temperature-induced degradation of GaN HEMT: An *in situ* heating study **⊕**⊘

Md Abu Jafar Rasel ⑩ ; Di Zhang; Aiping Chen; Melonie Thomas; Stephen D. House ⑩ ; Winson Kuo ⑩ ; John Watt ⑪ ; Ahmad Islam ⑩ ; Nicholas Glavin ⑩ ; M. Smyth ⑩ ; Aman Haque ➡ ⑩ ; Douglas E. Wolfe ⑩ ; Stephen J. Pearton ⑫



J. Vac. Sci. Technol. B 42, 032209 (2024) https://doi.org/10.1116/6.0003490







Cite as: J. Vac. Sci. Technol. B **42**, 032209 (2024); doi: 10.1116/6.0003490 Submitted: 17 March 2024 · Accepted: 11 April 2024 · Published Online: 26 April 2024







Md Abu Jafar Rasel,¹ Di Zhang,² Aiping Chen,² Melonie Thomas,¹ Stephen D. House,³ D Winson Kuo,² D John Watt,² Aman Haque,^{1,a)} Douglas E. Wolfe,⁶ Aman Haque,^{1,a)} Douglas E. Wolfe,⁶ Aman Haque,^{1,a)} Douglas E. Wolfe,⁶ Aman Haque,^{1,a)}

AFFILIATIONS

- Department of Mechanical Engineering, Pennsylvania State University, University Park, Pennsylvania 16802
- ²Center for Integrated Nanotechnologies (CINT), Los Alamos National Laboratory, New Mexico 87545
- Center for Integrated Nanotechnologies (CINT), Sandia National Laboratories, New Mexico 87185
- Sensors Directorate, Air Force Research Laboratory, Wright-Patterson AFB, Ohio 45433
- ⁵Materials and Manufacturing Directorate, Air Force Research Laboratory, Wright-Patterson AFB, Ohio 45433
- ⁶Department of Materials Science and Engineering, Pennsylvania State University, University Park, Pennsylvania 16802
- ⁷Department of Material Science and Engineering, University of Florida, Gainesville, Florida 32611

ABSTRACT

High-power electronics, such as GaN high electron mobility transistors (HEMTs), are expected to perform reliably in high-temperature conditions. This study aims to gain an understanding of the microscopic origin of both material and device vulnerabilities to high temperatures by real-time monitoring of the onset of structural degradation under varying temperature conditions. This is achieved by operating GaN HEMT devices *in situ* inside a transmission electron microscope (TEM). Electron-transparent specimens are prepared from a bulk device and heated up to 800 °C. High-resolution TEM (HRTEM), scanning TEM (STEM), energy-dispersive x-ray spectroscopy (EDS), and geometric phase analysis (GPA) are performed to evaluate crystal quality, material diffusion, and strain propagation in the sample before and after heating. Gate contact area reduction is visible from 470 °C accompanied by Ni/Au intermixing near the gate/AlGaN interface. Elevated temperatures induce significant out-of-plane lattice expansion at the SiN_x/GaN/AlGaN interface, as revealed by geometry-phase GPA strain maps, while in-plane strains remain relatively consistent. Exposure to temperatures exceeding 500 °C leads to almost two orders of magnitude increase in leakage current in bulk devices in this study, which complements the results from our TEM experiment. The findings of this study offer real-time visual insights into identifying the initial location of degradation and highlight the impact of temperature on the bulk device's structure, electrical properties, and material degradation.

Published under an exclusive license by the AVS. https://doi.org/10.1116/6.0003490

I. INTRODUCTION

Wide-bandgap devices, such as AlGaN-GaN high electron mobility transistors (HEMTs), ¹⁻¹⁴ have become increasingly popular because of several advantages over traditional silicon-based transistors in extreme environments, such as higher bandgap, lower intrinsic carrier concentration, excellent power handling capabilities, etc. ¹⁵ Next-generation radar systems, satellite communications, and high-frequency wireless communication devices require microwave power amplification and high-power, high-temperature applications. Temperature affects the GaN-based devices, such as UV

sensors as well as GaN HEMT.^{16–18} GaN HEMTs are used in harsh environments where traditional silicon-based transistors may not operate efficiently, making them suitable for downhole drilling, geothermal exploration, automotive for efficient power conversion, and space missions. The thermal stability of these structures and changes in stress related to thermal excursions are keys for stable operation. AlGaN/GaN HEMTs designed for room-temperature, high-power applications may experience device self-heating. This self-heating phenomenon can elevate the channel temperature

a) Author to whom correspondence should be addressed: mah37@psu.edu

beyond 300 °C, 19 a condition known to expedite device failure in high-power AlGaN/GaN transistors. The AlGaN/GaN/SiC structure exhibits superior thermal management and film quality compared to Si or sapphire substrates, attributed to SiC's higher thermal conductivity and reduced lattice mismatch. However, achieving highquality GaN has proven challenging due to the lattice mismatch and differing thermal expansion coefficients (TECs) between the epitaxial layer and the substrate. Although a very thin AlN layer is used to reduce the mismatch, TEC difference still poses a severe problem as it produces residual stress in the heterostructure. The disparity in the TEC among various layers can impact the device's mechanical and electrical performance while operating at elevated temperatures. While extensive experimental research 20-31 has explored the temperature-dependent degradation of GaN HEMTs, as far as our knowledge extends, no study has yet pinpointed the precise location where this degradation initiates solely due to high temperatures. Conducting an in situ transmission electron microscopy (TEM) study along with the electrical characterization of bulk devices can provide real-time insights into the performance degradation of GaN HEMTs under varying temperature conditions, which is the primary motivation of this study.

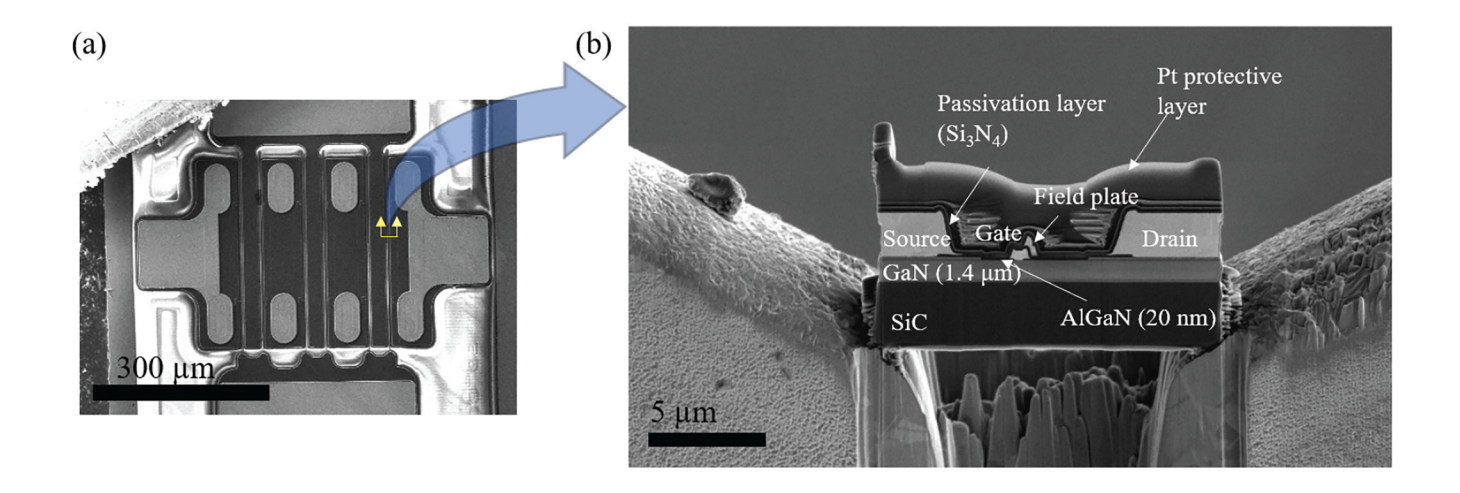
Various literature sources have reported on the hightemperature performances of GaN HEMTs with Si, SiC, and sapphire substrates, covering a temperature range from 25 to 500 °C. 20-24,29,32 All authors commonly observe a significant reduction in drain current density and transconductance with increasing temperature, attributed to the intrinsic scattering process and decrease in carrier mobility.²² The degree of reduction with temperature is dependent on the substrate and gate length used in the devices. It has been found in several studies that the GaN HEMT device shows good stability up to 300 °C21,22,33 even after 250h stressing,³³ and the device recovers its original properties when cooled down from 500 °C to room temperature.²³, ¹⁴ A change in gate metal color accompanied by a sharp decline in device performance is reported.²² The color alteration began at approximately 400 °C, indicating that device degradation results from gate metal alloying. An increase in leakage current due to the instability of Schottky contact is observed due to contact degradation by Au diffusion through the gate edge to the gate and AlGaN interface. 34,35 Maier et al. observed high leakage current and gate diode breakdown in GaN HEMT at 500 °C after 219h stressing.³³ Besides hightemperature operation experiment, a study³⁶ reported that postannealing of the device at 400 °C significantly improved the performance of AlGaN/GaN HEMTs with notable enhancements in breakdown voltages (from 7.5 to 187 V), elimination of kinks in device characteristics, and reduced trap presence, resulting in better uniformity and adjusted threshold voltages. These findings underscore the positive impact of postprocessing annealing on the DC, RF, and microwave power characteristics of GaN-based HEMTs. Their research was constrained to a maximum temperature of 400 °C, and they solely anticipated the Ni diffusion from the gate to AlGaN as a potential cause for the drop in drain current, lacking any additional experimental validation. Ni/Au metallization is commonly used as Schottky contact and is usually the primary cause of failure in high-temperature operations. The intermixing of Ni and Au is anticipated to occur at the Schottky contact. All these findings point out that the primary factor influencing failure is the

device processing technology and metallization scheme (ohmic and Schottky contact) rather than the stability of the heterostructure material. Moreover, biased devices exhibit more pronounced degradation from electromigration compared to their unbiased counterparts exposed to the same temperature environment.³³ Chowdhury et al. reported that stressed devices consistently developed crackand pit-shaped defects in the AlGaN/GaN crystal material under the drain-side edge of the gate, but unstressed devices did not show these features. The formation of these defects is consistent with the theory of damage from the inverse piezoelectric effect,³⁷ suggesting that the electrical degradation is a direct result of the formation of these defects. However, in strained heterostructures such as AlGaN/ GaN, the thermal and mechanical stresses resulting from mismatches in TEC and lattice parameters have the potential to cause premature material degradation. It has also been demonstrated that achieving device operation up to 900 °C is possible by employing a lattice-matched InAlN/GaN heterostructure and substituting the Au conductive overlay with Cu,³³ while operation at 1000 °C is attainable with refractory metal contacts, specifically Mo gates.²⁷ However, identifying a distinctive failure pattern in the device characteristics data or the postmortem analysis approach, where TEM analysis is conducted after device degradation, cannot provide an exact temperature of initiation of degradation. In situ TEM studies provide a powerful platform for real-time observation of dynamic processes at nanoscale in electronic devices.^{38–41} Here, we introduce an in situ heating study within TEM to observe real-time Schottky metal degradation at elevated temperatures. Furthermore, the bulk form of the device undergoes heating in a comparable environment to assess whether the degradation observed in the TEM sample is mirrored in the electrical properties of the bulk sample.

II. MATERIALS AND METHODS

In this study, we chose to utilize commercially available Cree

multi-finger HEMT dies (CGH60008D, Wolfspeed, rated at 6W, 18 GHz, and 40 V) as shown in Fig. 1(a). The manufacturer's provided layer structure, as shown in Fig. 1(b), includes approximately $a \approx 20 \text{ nm Al}_{0.22} Ga_{0.78} N$ barrier, $a \approx 1 \text{ nm-thick AlN}$ interlayer, a 1.4 µm GaN buffer, and a 100 µm 4H-SiC substrate, with a gate length of Lg = $0.25 \,\mu\text{m}$. The formation of Ohmic contacts (Ti/Al/ Ni/Au) is achieved directly on the upper AlGaN layer. In addition, Schottky metal gate electrodes are created by depositing Ni/Au metallization, and a laterally extended gate metallization is applied to reshape and redistribute the strong peak electric fields during device operation. For in situ heating within the TEM, a lamella is prepared from the bulk GaN HEMT device using Ga+ focused ion beam (FIB), as illustrated in Fig. 1(a), and placed it on a molybdenum refractory metal grid. To reduce beam-induced damage, the final thinning steps involve low-kV (5 kV) thinning with a 48 pA current. TEM and EDX experiments were conducted using a 300 kV Tecnai G2 F30 S-TWIN, equipped with scanning transmission electron microscopy high-angle annular dark field (STEM HAADF) capabilities, offering a resolution of 0.17 nm. We employed the Gatan model 652 double-tilt heating holder, equipped with a water-cooled Tantalum furnace capable of reaching temperatures up to 1000 °C as demonstrated in Fig. 1(c). This furnace features an encapsulated heater connected to two terminals



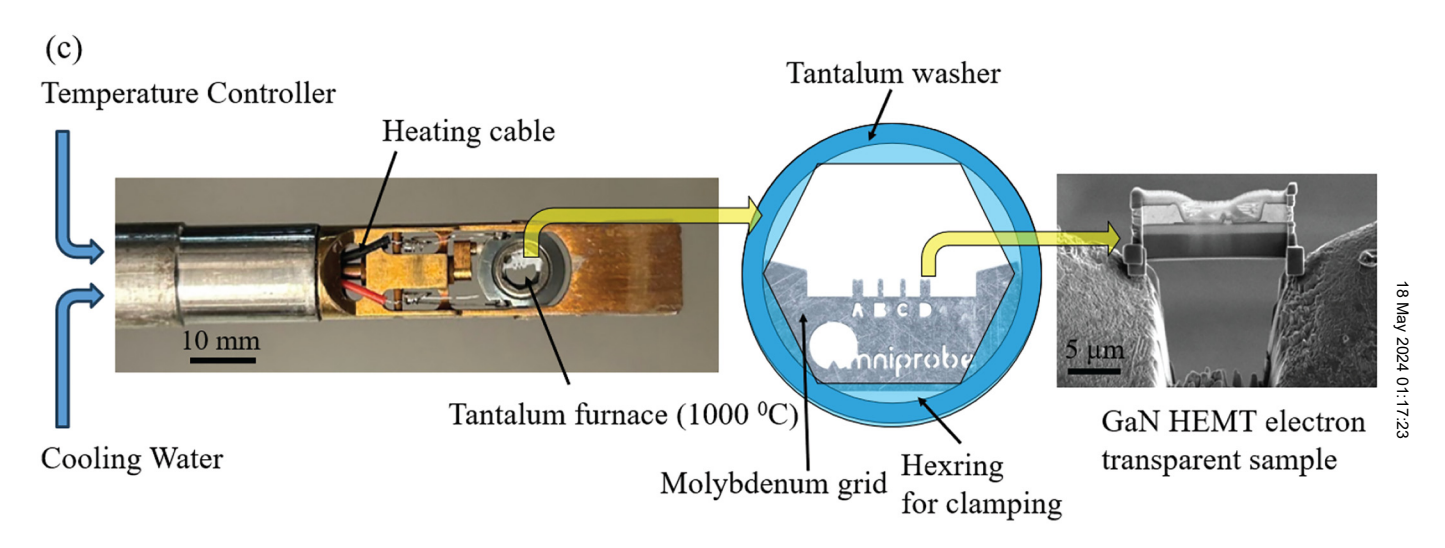


FIG. 1. (a) SEM image of a bulk GaN HEMT die. The arrow pointing outward from an active channel out of six and the double headed arrow shows the direction of FIB cut. (b) A cross-sectional cut was made inside the SEM image using a Ga+ FIB and placed on a molybdenum (Mo) TEM grid, exposing the terminals, substrate, and the conductive channel material. (c) The Gatan heating holder, equipped with a Tantalum furnace, houses a Mo grid that contains a TEM electron-transparent lamella with a thickness of approximately 100 nm.

for the current supply, and it also incorporates a platinum-13% rhodium thermocouple, securely spot-welded to the furnace body to monitor the furnace temperature. All connections are routed through a vacuum feed-through to the model 901 SmartSet hot stage temperature controller, which manages water pumping when the temperature exceeds 500 °C. The heating process was conducted in a "Ramp" mode with a ramping rate of 10 °C/min.

III. RESULTS AND DISCUSSION

Before ramping up the temperature, TEM imaging is conducted at multiple locations, especially focusing on the gate, source, and drain regions for each 100 °C temperature increment up to

400 °C. This is performed to assess and compare any changes following the temperature increase. Specific attention is placed on the AlGaN/GaN interface, which serves as the conducting channel in the device's bulk state. High-resolution TEM (HRTEM), energy-dispersive x-ray spectroscopy (EDS), and scanning transmission electron microscopy are conducted both in the initial pristine state and subsequently after each 100 °C temperature increment, as well as during any observable changes. Additionally, video recordings are made during the intervals.

Figure 2(a) shows a STEM image of the cross section of the GaN HEMT encompassing the gate, drain, and source regions. The Ni gate contact material is positioned directly on top of the AlGaN layer [Fig. 2(b)], and the gate and drain material layers [Fig. 2(c)]

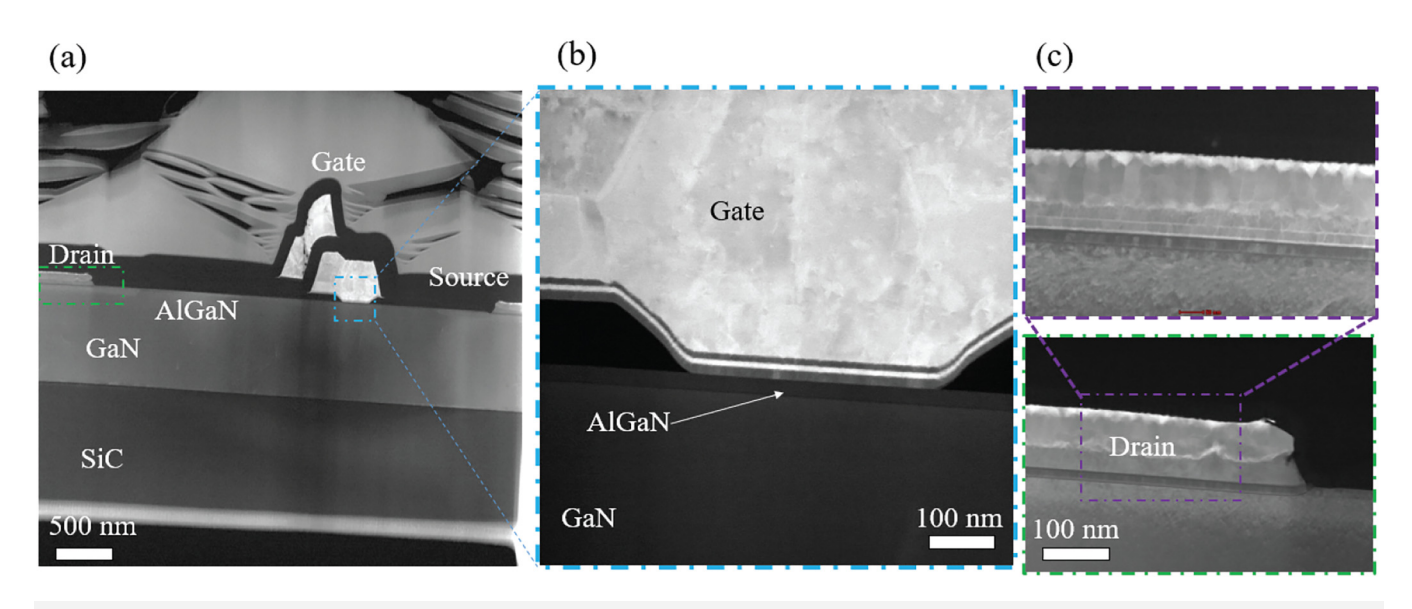


FIG. 2. (a) Scanning transmission electron microscope (STEM) images of the GaN HEMT lamella, displaying the (b) gate and (c) drain terminals in their initial pristine state, before undergoing any heating. The gate metal is Ni, while the source (not shown here) and drain terminals consist of Ti metal placed directly on the AlGaN/GaN semiconductor layer.

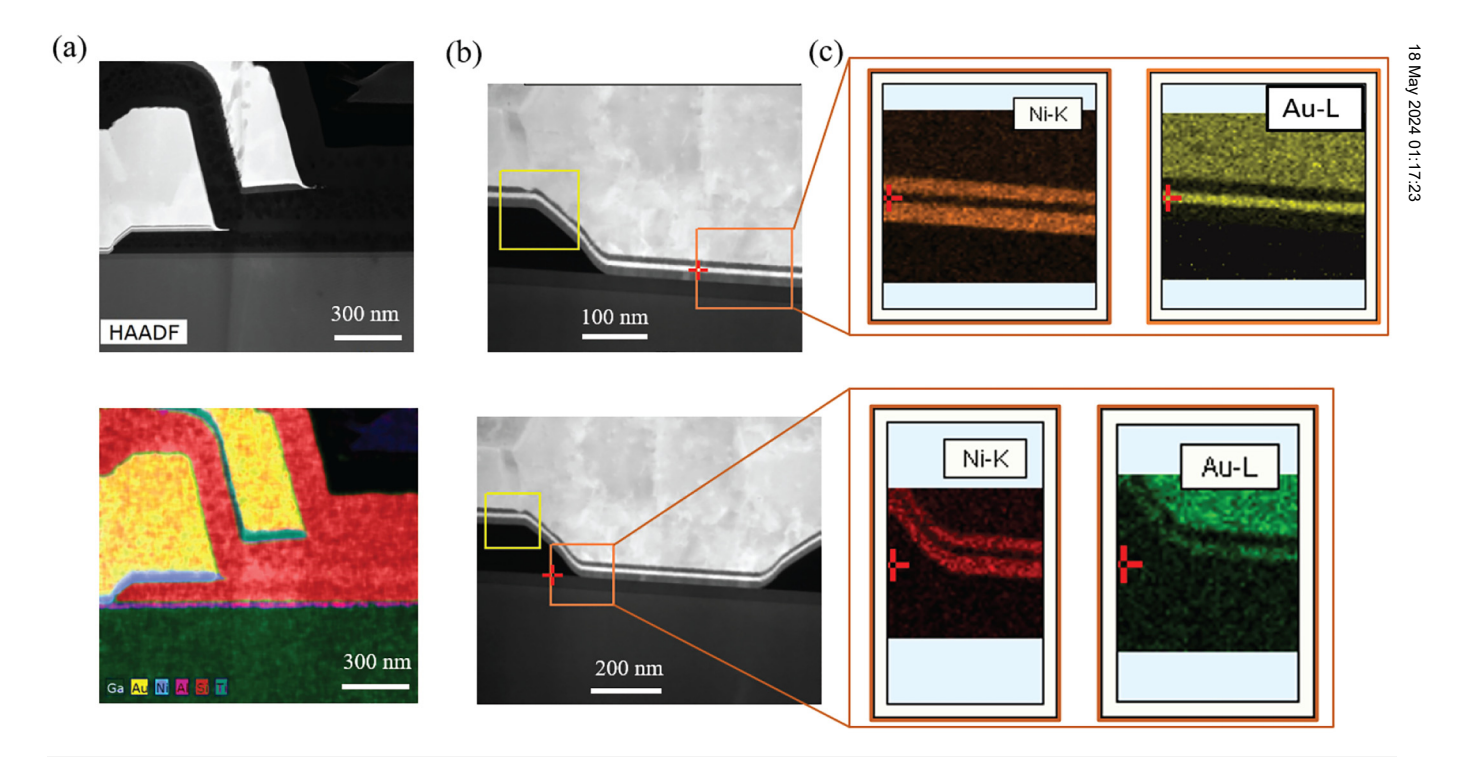


FIG. 3. (a) HAADF image provides a view of the gate and the AlGaN/GaN region, while the accompanying energy-dispersive x-ray spectroscopy (EDS) map reveals the elemental distribution. In the EDS map, the red-colored area represents the passivation layer of SiN_x. (b) and (c) A closer view of the gate contact reveals Ni/Au metallization, a configuration that is further corroborated by EDS mapping. The fine boundary between each metal layer is clearly discernible in its pristine state.

are distinctly visible in their pristine state. The area beneath the drain contact displays a slight roughness, attributed to variations in the milling rates of the metal and semiconductor during the FIB milling process, creating a "curtaining effect" in the milled region. 42 Additionally, the abrupt junction in the metal/semiconductor contact region arises from nonuniform metal diffusion during 850 °C source/drain activation annealing. Considering that GaN and SiC materials have higher melting points than the contact terminal material, our primary focus was directed toward the latter during imaging and video recording.

EDS at room temperature in the gate region shows the compositional map [Fig. 3(a)] of the GaN HEMT lamella, with a particular focus on the gate contact area, where a sandwiched structure of Ni and Au layers is discernible from Figs. 3(b) and 3(c). Our mapping suggests that gate metallization is structured in a Ni/Au/Ni/Au sequence.

Before taking any measurements, we implemented a 1-h waiting period to prevent drift during high-resolution imaging. Up to 300 °C, there were no apparent changes in the device structure near the metal-semiconductor contacts as depicted in Figs. 4(a)-4(c). Additionally, EDS analysis, which is not presented here, did not reveal any evidence of material diffusion. However, starting at 300 °C, we observed a slight increase in brightness of the gate metal and AlGaN interface, with the effect becoming more pronounced as the temperature reached 400 °C as displayed in Fig. 4(d). Furthermore, starting at 300 °C, we observed the edge of the gate material diffusing, beginning from the Au metal region and extending toward the Ni/Au region. By the time we reached 400 °C, we noted alloying and the complete disappearance of each individual layer of the metal stack. The initial diffusion of the Ni/Au layer at the edge, rather than at the AlGaN/Ni/Au contact region, can be attributed to the fact that the edge region is in contact with a material of relatively lower thermal conductivity (SiNx) along with a rough interface between them. The STEM image provides enhanced contrast, revealing the disassociation of the Ni/Au layers as Ni metal coalesces with other Ni atoms and increases in area and mobility, as illustrated in Figs. S1(a) and S1(b).⁵⁰ See supplementary material⁵⁰ for more images of degradation in GaN HEMT.

Around 470 °C, it becomes evident that the gate contact area near the drain terminal is diminishing due to the diffusion of Ni from the metal stack, as depicted in Fig. 5(a) with an increase in brightness. Notably, there are no signs of degradation in the source and drain contacts at 500 °C. A prior in situ study conducted within TEM revealed that under high current density, the drain metal contact became mobile and mixed with more Au metal, which subsequently diffused through the AlGaN and GaN layers to the substrate due to electromigration. 41 However, our examination using low-resolution scanning transmission electron microscopy (STEM) did not reveal any such formation or diffusion into the AlGaN layer since biasing was not applied. Instead, Ni at the gate edge appears to have separated and relocated to an adjacent area, forming a separate Ni metal region within the gate region. We identified the atomic diffusion of Au and Ni metals through EDS line spectra as illustrated in Fig. 5(b), collected at various locations spanning the gate and AlGaN interface, and subsequently averaged. The analysis reveals the presence of both Au and Ni metals penetrating deeply into the AlGaN layer, with Ni being more abundant compared to Au. The degradation of the gate contact can lead to several issues, including a reduction in the barrier height, an increase in leakage current, and the formation of local hotspots during device operation. These factors collectively pose a risk to the device's reliability. Even though our experiment was conducted in device's off-state mode, it offers valuable insights into the potential consequences during device operation. Specifically, it highlights that if the channel temperature surpasses 500 °C, there is a risk of the gate material diffusing away. This risk is particularly pronounced in the gate edge near the drain contact area, which is identified as a hotspot with the highest electrical field (Fig. 6).

EDS spectra after 500 °C also show significant intermixing of ²³ Ni and Au as illustrated in Fig. 5(c). The Au map clearly shows that it has reached near the AlGaN layer through the Ni layer, and

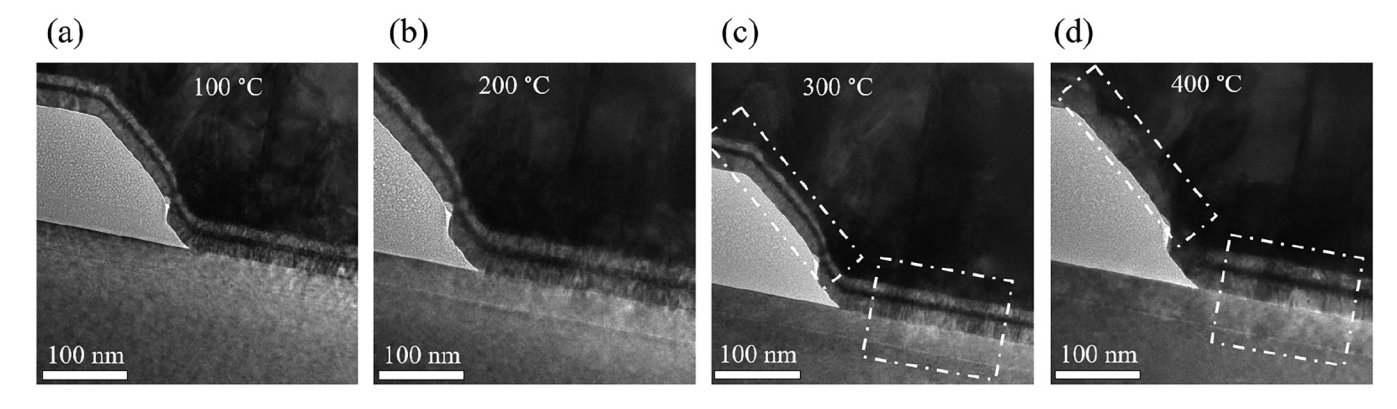
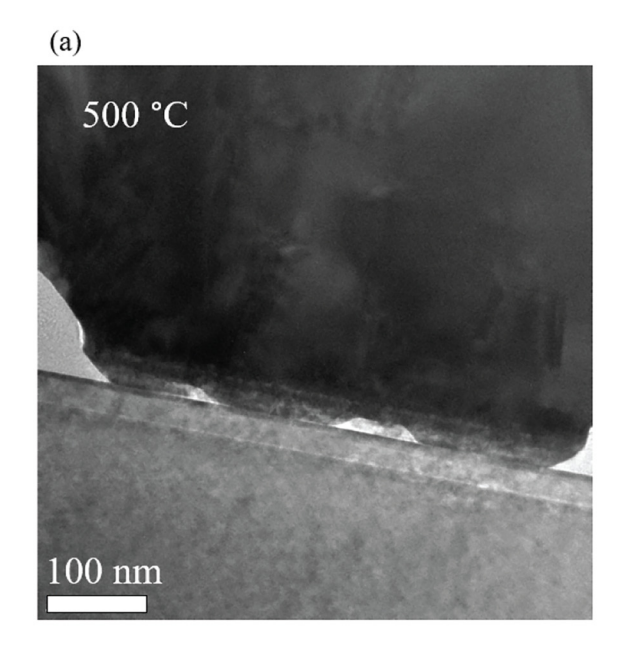


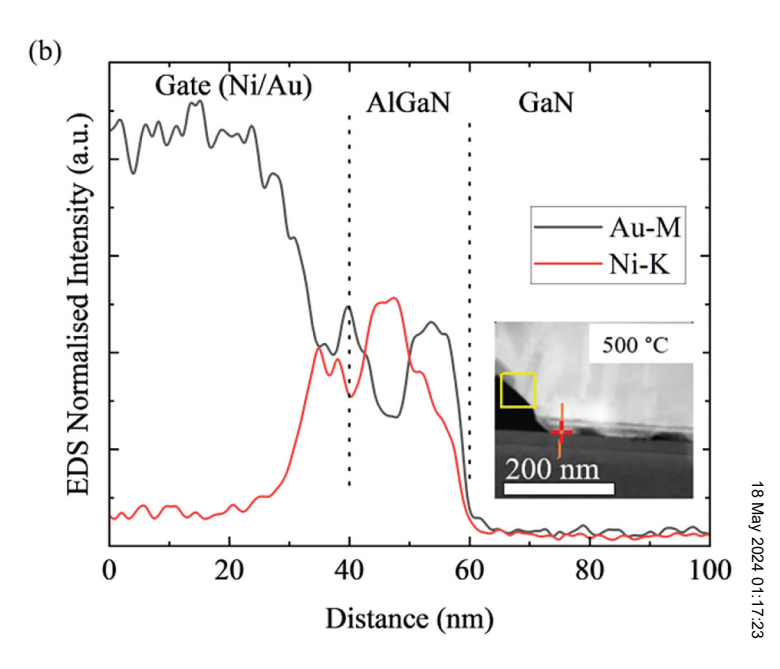
FIG. 4. These TEM images depict the gate edge at every 100 °C temperature increment up to 400 °C. (a) and (b) At 100 and 200 °C, no noticeable changes are detected. (c) At 300 °C, the gate/AlGaN interface begins to exhibit signs of degradation, with slight whitening in that area, indicating the mixing/alloying of the gate material. (d) At 400 °C, the whitening intensifies, indicating the alloying of the gate edge material, marked within the white box.

the Ni Schottky contact has become an Au Schottky contact. The Schottky barrier height of Au on GaN is comparable to that of Ni on GaN (Au: 5.1 eV versus Ni: 5.15 eV). ⁴³ However, the Au Schottky gate exhibits instability during high-temperature stress, leading to a decrease in barrier height and elevated leakage current. ³⁴ Au also does not stick well with AlGaN. Due to poor adhesion between Au and AlGaN, the gate control of the two-dimensional electron gas (2DEG) can be compromised. It is important to note that the brighter area near the orange box in Fig. 5(c)

is due to contamination buildup during STEM-EDS imaging and is not indicative of Au diffusion.

High-resolution transmission electron microscopy (HRTEM) images were taken at 100 °C increments, revealing that there is no notable deterioration in crystal quality up to 480 °C. Given the considerably higher melting temperatures of GaN and SiC, no degradation is expected at 480 °C. The lattice expansion resulting from heating can alter the strain propagation within the conductive 2DEG layer positioned between AlGaN and GaN, potentially





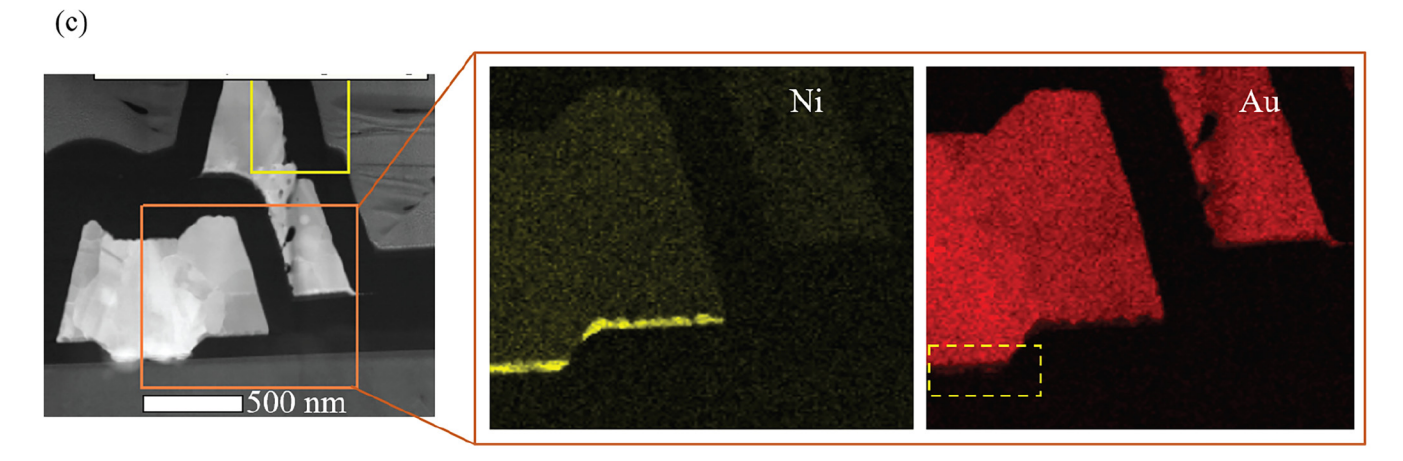
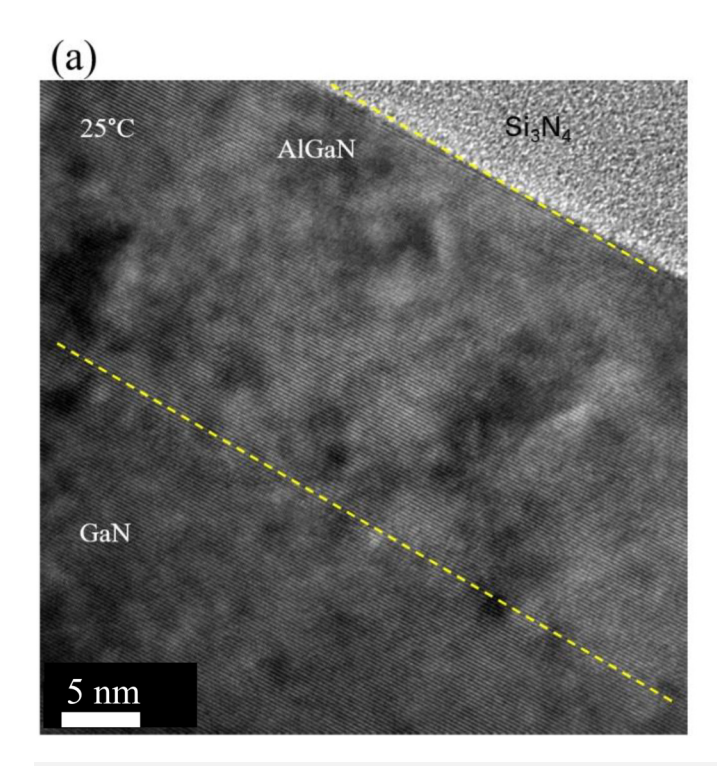


FIG. 5. (a) TEM and STEM images at 500 °C, illustrating the reduction in the gate contact area due to the vaporization of the gate metal at the Ni/AlGaN interface. (b) EDS line spectra across the Gate/AlGaN/GaN interface taken in multiple sites and averaged afterward. (c) An EDS map that further validates the mixing of Ni and Au at the interface, with no distinct boundary being visible anymore. Additionally, the Au map indicates that Au has diffused near the interface highlighted using a dotted



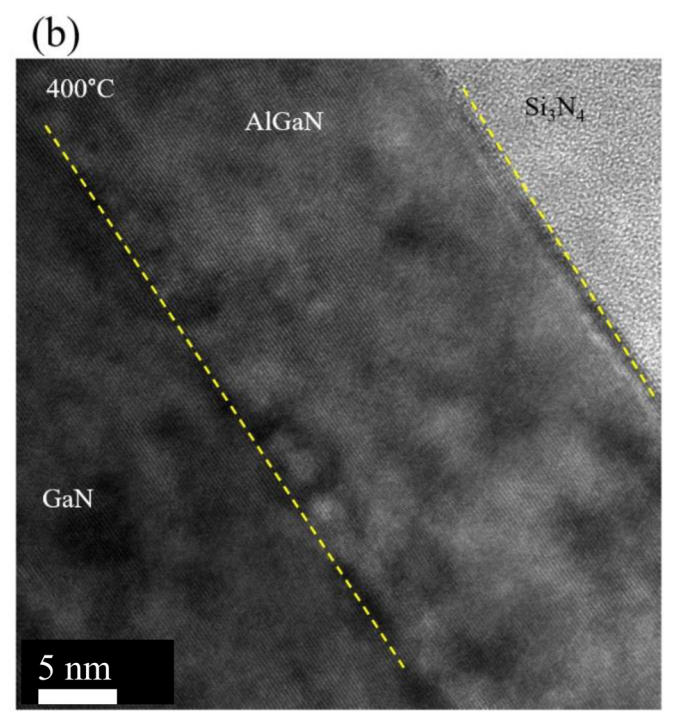


FIG. 6. HRTEM images of SiN_x/GaN/AlGaN interface at (a) 25 and (b) 400 °C. While certain areas in the GaN region appear blurrier after 400 °C, there is no significant crystal deterioration observed in the AlGaN and GaN regions.

leading to degradation in the device's electrical performance. Additionally, geometric phase analysis (GPA) was performed based on the HRTEM images along in-plane (ε_{xx}) and out-of-plane (ε_{yy}) directions to visualize the lattice strains within the device layer stack at different temperatures. Figure 7 shows the HRTEM images of the SiN_x/GaN/AlGaN interface and the corresponding GPA strain maps at 300, 400, and 480 °C, respectively. The inset in the HRTEM images is the fast Fourier transform power spectrum with labeled g-vectors used for phase calculation. The reference lattices were taken from the clean and undistorted GaN region in all the HRTEM images. Here, ε_{xx} and ε_{yy} indicate the in-plane and out-of-plane strain directions at the SiN_x/GaN/AlGaN interface. It can be seen that the intensity of the in-plane strains at the GaN/AlGaN interface [Figs. 7(d)-7(f)] are consistent and less impacted by the rise of the temperature. In contrast, by increasing the temperature from 300 to 480 °C, the out-of-plane strain maps [Figs. 7(g)-7(i)] show increasingly distinguishable contrast in the GaN and AlGaN phases, indicating that the lattice expansion is more noticeable along the out-of-plane direction to the interface. We have added the line intensity profiles of the out-of-plane (ε_{vv}) strain maps of the film at different temperatures in Fig. S2.50

To compare the observed temperature degradation inside the TEM to traditional bulk device performance, we also subjected a bulk GaN HEMT sample to a heating process inside a vacuum chamber, raising the temperature in 100 °C increments up to 600 °C over the course of 1 h. It is anticipated that the degradation

observed in the gate region of the ~100 nm-thin lamella and in the bulk sample will differ due to variations in the surface-to-volume ratio and boundary conditions in these two scenarios. After each 100 °C temperature increment during 1-h high-temperature stress, we conducted measurements of the device's electrical transport properties, especially gate leakage to identify any indication of permanent degradation. It is important to highlight that these electrical measurements were performed at room temperature following cooling of the device.

Figure 8(a) depicts a pivotal device parameter, namely, transconductance (Gm), which quantifies the relationship between changes in the device's output current (drain current) and changes in its input voltage (gate-source voltage). We have observed a shift in the peak Gm value, which corresponds to a threshold voltage shift. This shift is initially positive, rising to 200 °C, and subsequently becomes negative, dropping from -2.8 to -3.1 V. The $G_{\rm m}$ value reaches the highest value at 300 °C (92% increase), primarily due to the high forward saturation current observed at this temperature. Subsequently, there is a decline in the Gm value, although it remains 48% higher than that of the pristine device. Regarding leakage current, we have observed a consistent and gradual increase. This increase becomes more pronounced at temperatures of 500 and 600 °C, where we observe a significant one and half order of magnitude increase in leakage current. The increase in leakage current is an obvious indication of Schottky contact degradation at higher temperatures. The initial increase in

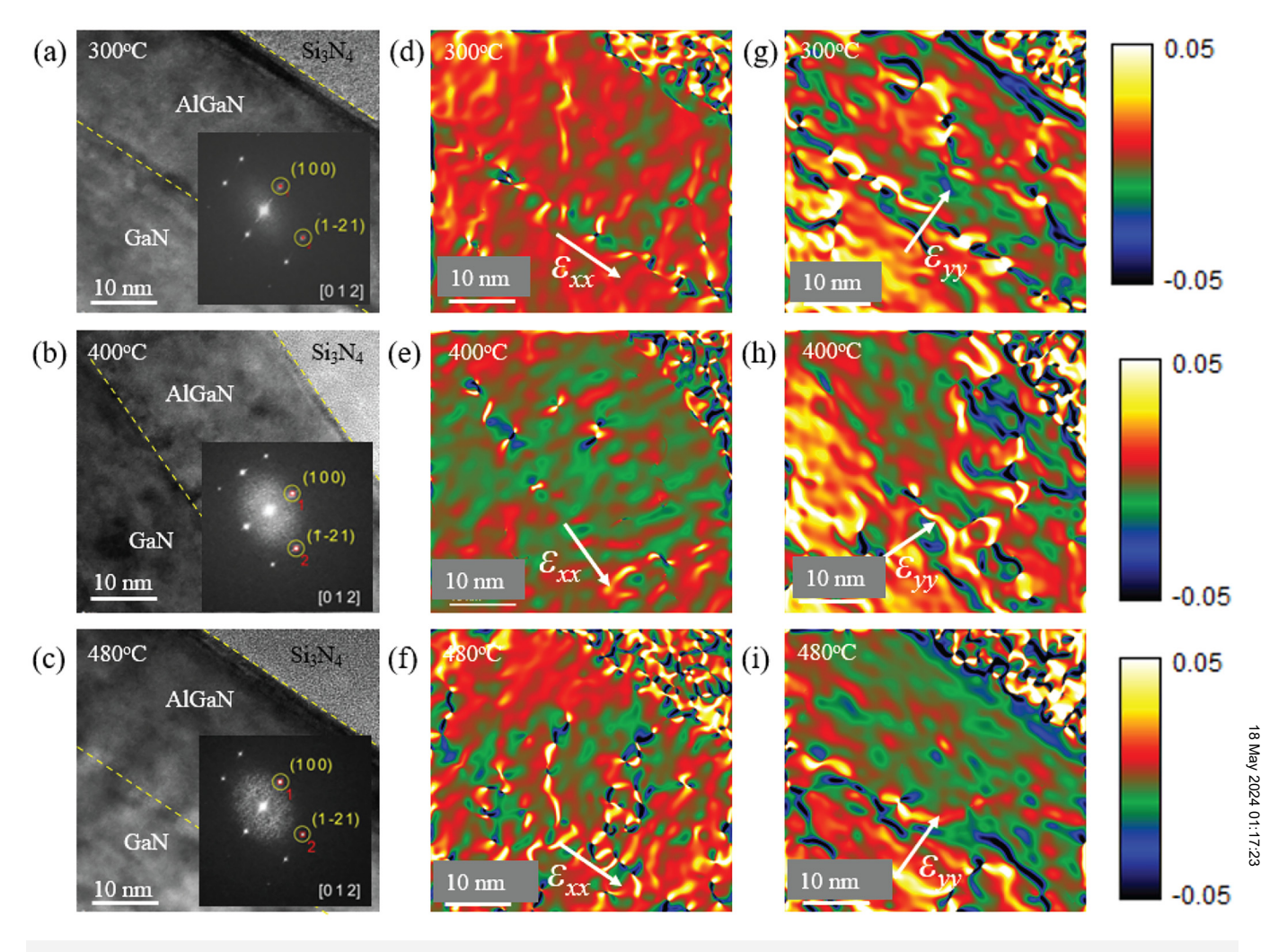
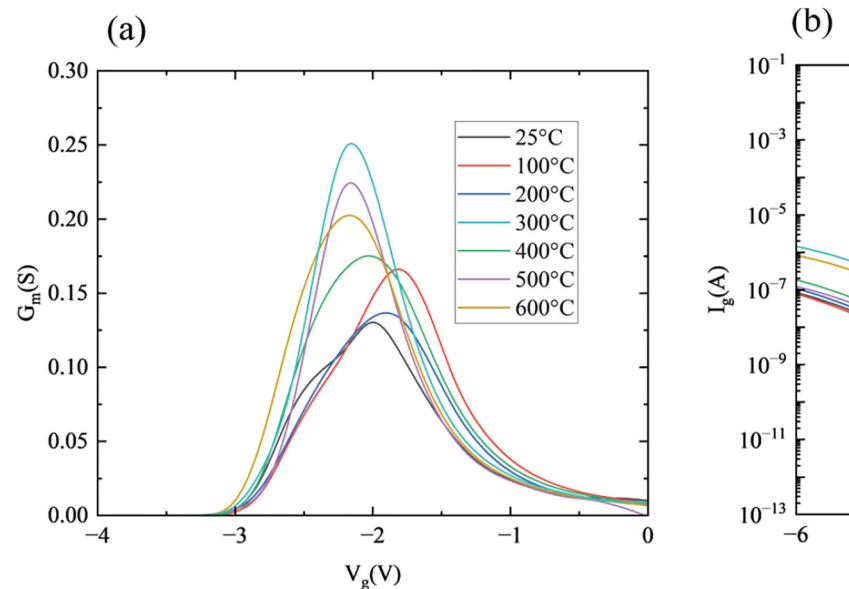


FIG. 7. (a)–(c) HRTEM of GaN HEMT lamella at 300, 400, and 480 °C taken at the [1,0,-1,0] zone axis. GPA map where the strain directions are adjusted to make sure we get the (d)–(f) in-plane and (g)–(i) out-of-plane (with respect to the interface) direction of strains in the film.

transconductance indicates that annealing is beneficial for devices up to 300 °C. As AlGaN has smaller CTE than GaN,46 higher tensile strain is exerted from both SiNx and GaN layers. This tensile strain enhances the band bending effect in the AlGaN layer, elevating the number of surface states with donorlike characteristics above the Fermi level, ultimately leading to an augmented electron density within the 2DEG. 47 Such an increase is reported at 600 °C in contrast to our device, where it occurs at lower temperatures, and this disparity can be ascribed to variations in device design and the residual strain introduced during the fabrication process. However, beyond 300 °C, the tensile strain surpasses its critical threshold, initiating strain relaxation that can result in a decrease in 2DEG density due to the creation of additional defects or structural cracks. Additionally, the diffusion of gold or nickel into the AlGaN layer can effectively reduce the thickness of the AlGaN layer, thereby increasing the threshold voltage in the device.³⁶ A TEM sample has been prepared from the bulk devices after annealing at 500 °C to examine potential gate metal diffusion. In Fig. 9(a), the EDS line spectra reveal that the metal stack maintained its layered structure. However, discernible Au diffusion through the AlGaN layer has been identified, further confirming the degradation of gate characteristics. Au diffused to the GaN layer, while Ni showed very little or no diffusion. This preferential diffusion of Au can be attributed to the significant difference in electronegativity between Au and Ga, which facilitates a stronger bonding interaction between Au and GaN compared to that between Ni and GaN.⁴⁸ The STEM HAADF image depicted in Fig. 9(b) illustrates a certain level of intermixing between Ni and Au in the edge region of the gate. A closer examination of the highlighted dotted region confirms this intermixing. However, it is important to note that no significant intermixing is observed in the gate contact region in contrast to our observations in the TEM heating experiment.



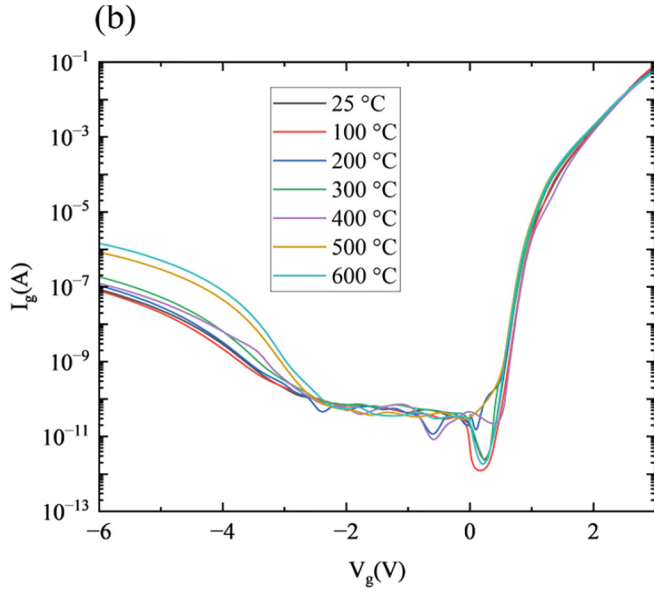
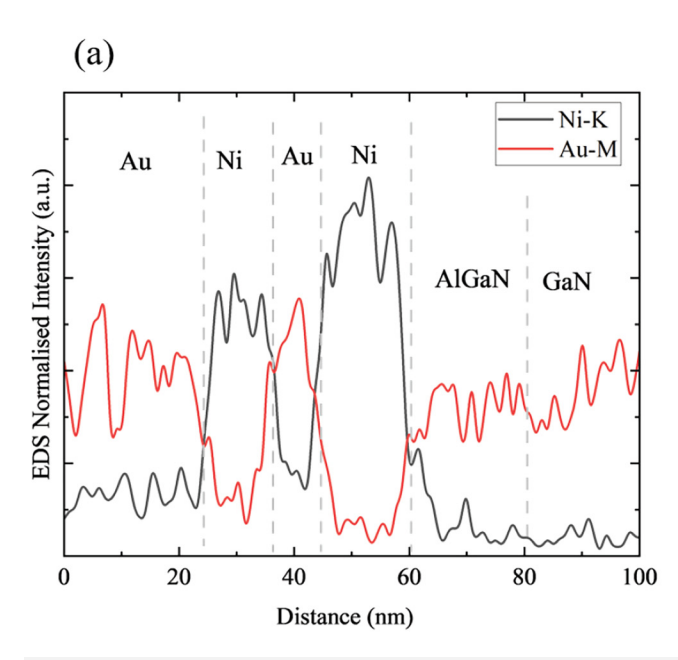


FIG. 8. (a) Transconductance derived from transfer characteristics at V_{ds} = 1 V as a function of annealing temperature. (b) Forward and reverse leakage current characteristics tics of Ni/Au Schottky contact as a function of annealing temperature.

A recent investigation³² reveals the disappearance of Ni from the gate contact and its substitution with Au in their bulk devices after exposure to 500 °C. It is noteworthy that their devices were operated at 500 °C, unlike our case where we solely annealed the

sample. This implies that high temperatures, coupled with device operation, expedite the degradation of the device. The presence of a whitish region at the gate edge, as indicated by the arrow, resembles our TEM heating experiment after 470 °C.

(b)



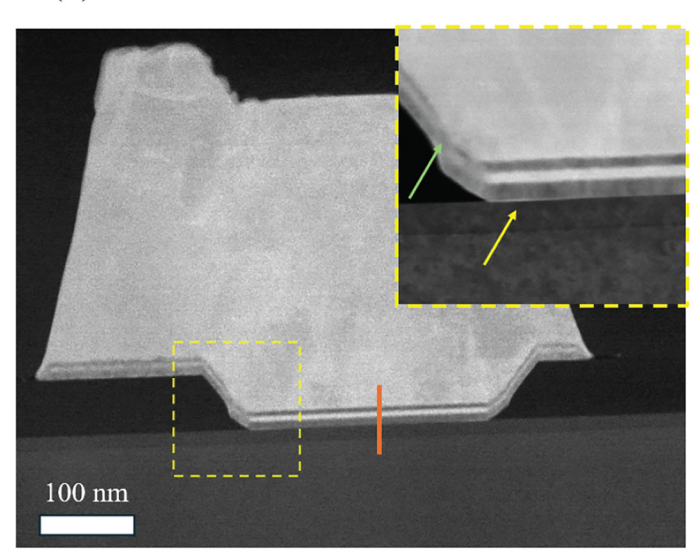


FIG. 9. (a) EDS line spectra across the Gate/AlGaN/GaN interface [the orange line in Fig. 8(b)] taken in multiple sites and averaged afterward. The TEM sample was prepared from a bulk GaN HEMT device that underwent annealing at 500 °C for an hour. (b) The STEM HAADF image of the gate area of the same bulk device with a dotted box shows a closer look at the edge.

We also increased temperatures beyond 500 °C in TEM samples to observe degradation in other terminals. See supplementary material⁵⁰ for more images of degradation at higher temperatures in GaN HEMT. Figure S3(a)⁵⁰ clearly illustrates the degradation of the source and drain contacts, which becomes evident at temperatures exceeding 600 °C, as observed in comparison to their pristine condition in Fig. 2(c). Beyond 600 °C, they undergo alloying, resulting in the disappearance of visible features. Notably, the Ti/GaN interface experiences intermixing and surface roughening after 600 °C. Ni metal islands begin to coalesce into larger islands within the Au metal and migrate toward the edge of the gate, as depicted in Figs. S3(b) and S3 (c).⁵⁰ By 800 °C, approximately half of the gate metal had disappeared. Given that melting or vaporization at 800 °C is unlikely, we hypothesize that the gate metals underwent recrystallization/densification to form more stable Au/Ni grains. Figure S3(d)⁵⁰ shows increased brightness in the gate area, which could result from thicker gate regions, as intensity scales linear with thickness. It is possible that Au and Ni diffused and underwent densification, leading to a thicker layer. The bulk device exhibited comparable gate contact diffusion and visible signs of gate metal degradation, including field plate melting above the gate contact at 800 °C as shown in Figs. S4 (a)-S4(c). Additionally, a gap in the source and drain contacts is formed due to metal evaporation or migration, leading to a complete loss of current output from the device.

The long-term reliability and stable operation at high temperatures must be ensured to address the increasing power density and reduced size of the GaN-based electronic power devices. Efficient thermal management techniques, such as advanced heat sinks or using diamond (which has six times higher thermal conductivity than SiC) as a heat spreader, can help minimize peak temperatures during both regular device operation and operation in high-temperature environments. Our study suggests that optimizing the design of gate and field plate structures, coupled with an efficient heat spreader, is crucial in achieving reliability of devices in extreme environments. Metal migration stands as a primary temperature limitation, and the incorporation of new metal stacks holds the potential to increase the operating temperature. To prevent thermal degradation in GaN HEMTs, one effective strategy is to incorporate a diffusion barrier between the gate and the AlGaN barrier. This can help reduce gate leakage by minimizing the migration of materials across interfaces.

IV. CONCLUSION

In conclusion, this study provides crucial insights into the temperature-dependent degradation mechanisms of GaN HEMTs, shedding light on their behavior under extreme conditions. The investigation, conducted through in situ transmission electron microscopy (TEM), reveals that the gate material starts to degrade at temperatures as low as 300 °C, with significant alloying and layer disappearance observed at 400 °C. Notably, the gate material starts diffusing away after 470 °C, and atomic diffusion of Au and Ni into the AlGaN layer was detected through EDS mapping. GPA reveals consistent in-plane strains at the GaN/AlGaN interface, while out-of-plane strains exhibit distinguishable contrast, indicating notable lattice expansion along the out-of-plane direction with increasing temperature. Furthermore, the investigation of bulk GaN

HEMT devices complements these findings, as it demonstrates that similar degradation processes occur, leading to gate contact diffusion/alloying, field plate degradation, and the creation of gaps in the source and drain contacts, ultimately resulting in a complete loss of current output at 800 °C. Almost two orders of magnitude increase in leakage current and threshold voltage shift are observed at temperatures higher than 500 °C. By employing advanced heat spreader materials and optimizing gate designs, the heat generated in the high-temperature environment can be effectively dissipated, preventing temperature spikes that may compromise the reliability of GaN HEMTs.

ACKNOWLEDGMENTS

The study was supported by the Defense Threat Reduction Agency (DTRA) as part of the Interaction of Ionizing Radiation with Matter University Research Alliance (IIRM-URA) under Contract No. HDTRA1-20-2-0002. A.H. acknowledges support from the U.S. National Science Foundation (ECCS # 2015795). N.G. gratefully acknowledges support from Air Force Office of Scientific Research under Grant No. FA9550-24RYCOR011. This work was performed, in part, at the Center for Integrated Nanotechnologies, an Office of Science User Facility operated for the U.S. Department of Energy (DOE) Office of Science. Sandia National Laboratories is a multi-mission laboratory managed and operated by National Technology & Engineering Solutions of Sandia, LLC, a wholly owned subsidiary of Honeywell International, Inc., for the U.S. DOE's National Nuclear Security International, Inc., for the U.S. DOE'S NATIONAL NUCLEAR SECURTY
Administration under Contract No. DE-NA-0003525. The views of expressed in the article do not necessarily represent the views of the U.S. DOE or the United States Government.

AUTHOR DECLARATIONS

Conflict of Interest

Conflict of Interest

The authors have no conflicts to disclose.

Author Contributions

Md Abu Jafar Rasel: Data curation (equal); Formal analysis (equal); Investigation (equal); Methodology (equal); Validation (equal); Visualization (equal); Writing - original draft (equal). Di Formal analysis (equal); Investigation Zhang: (equal); Methodology (equal); Validation (equal); Writing - review & editing (equal). Aiping Chen: Formal analysis (equal); Investigation (equal); Methodology (equal); Validation (equal); Writing - review & editing (equal). Melonie Thomas: Data curation (equal); Formal analysis (equal); Investigation (equal); Methodology (equal); Validation (equal); Visualization (equal); Writing - review & editing (equal). Stephen D. House: Investigation (equal); Methodology (equal); Resources (equal); Validation (equal); Writing – review & editing (equal). **Winson Kuo:** Investigation (equal); Methodology (equal); Resources (equal); Validation (equal); Writing - review & editing (equal). John Watt: Investigation (equal); Methodology (equal); Project administration (equal); Resources (equal); Validation (equal); Writing - review & editing (equal). Ahmad Islam: Formal analysis (equal); Investigation (equal); Methodology (equal); Validation

(equal); Writing - review & editing (equal). Nicholas Glavin: Funding acquisition (equal); Investigation (equal); Methodology (equal); Validation (equal); Writing - review & editing (equal). M. Smyth: Formal analysis (equal); Methodology (equal); Resources (equal); Validation (equal); Writing - review & editing (equal). Aman Haque: Conceptualization (equal); Formal analysis (equal); Funding acquisition (equal); Investigation (equal); Methodology (equal); Project administration (equal); Supervision (equal); Validation (equal); Writing - review & editing (equal). Douglas E. Wolfe: Conceptualization (equal); Funding acquisition (equal); Investigation (equal); Project administration (equal); Validation (equal); Writing - review & editing (equal). Stephen J. Pearton: Conceptualization (equal); Formal analysis (equal); Funding acquisition (equal); Investigation (equal); Methodology (equal); Project administration (equal); Validation (equal); Writing review & editing (equal).

DATA AVAILABILITY

The data that support the findings of this study are available from the corresponding author upon reasonable request.

REFERENCES

- ¹M. Meneghini et al., J. Appl. Phys. **130**, 181101 (2021).
- ²K. J. Chen, O. Häberlen, A. Lidow, C. lin Tsai, T. Ueda, Y. Uemoto, and Y. Wu, IEEE Trans. Electron Devices. **64**, 779 (2017).
- ³H. Fu, K. Fu, S. Chowdhury, T. Palacios, and Y. Zhao, IEEE Trans. Electron Devices. **68**, 3200 (2021).
- ⁴H. Amano et al., J. Phys. D: Appl. Phys. 51, 163001 (2018).
- ⁵F. Roccaforte, G. Greco, P. Fiorenza, and F. Iucolano, Materials. **12**, 1599 (2019).
- ⁶J. Ballestín-Fuertes, J. Muñoz-Cruzado-Alba, J. F. Sanz-Osorio, and E. Laporta-Puyal, Electronics **10**, 677 (2021).
- ⁷J. Wei, G. Tang, R. Xie, and K. J. Chen, Jpn. J. Appl. Phys. **59**, SG0801 (2020).
- ⁸J. R. Kumar, H. V. Du John, I. BinolaKJebalin, J. Ajayan, and D. Nirmal, Microelectron. J. **140**, 105951 (2023).
- ⁹N. Keshmiri, D. Wang, B. Agrawal, R. Hou, and A. Emadi, IEEE Access. 8, 70553 (2020).
- ¹⁰B. Romanczyk, W. Li, M. Guidry, N. Hatui, A. Krishna, C. Wurm, S. Keller, and U. K. Mishra, IEEE Electron Device Lett. 41, 1633 (2020).
- ¹¹S. Kargarrazi, A. S. Yalamarthy, P. F. Satterthwaite, S. W. Blankenberg, C. Chapin, and D. G. Senesky, IEEE J. Electron Devices Soc. 7, 931 (2019).
- ¹²Y. Ando, H. Takahashi, Q. Ma, A. Wakejima, and J. Suda, IEEE Trans. Electron Devices **67**, 5421 (2020).
- ¹³E. Zanoni et al., Phys. Status Solidi A 219, 2100722 (2022).
- ¹⁴A. I. Emon, A. B. Mirza, J. Kaplun, S. S. Vala, and F. Luo, IEEE J. Emerg. Sel. Top. Power Electron. 11, 2702–2729 (2022).
- ¹⁵P. G. Neudeck, R. S. Okojie, and L.-Y. Chen, Proc. IEEE **90**, 1065 (2002).
- 16L. Yang et al., Appl. Phys. Lett. 120, 091103 (2022).
- ¹⁷S. Shin, H. Lee, and H. So, IEEE Access **9**, 54184 (2021).
- ¹⁸K. Baek, S. Shin, and H. So, Eng. Appl. Artif. Intell. 123, 106309 (2023).
- ¹⁹J. Kuzmik, R. Javorka, A. Alam, M. Marso, M. Heuken, and P. Kordos, IEEE Trans. Electron Devices 49, 1496 (2002).
- ²⁰N. Maeda, T. Saitoh, K. Tsubaki, T. Nishida, and N. Kobayashi, Jpn. J. Appl. Phys. 38, L987 (1999).
- ²¹R. Gaska, Q. Chen, J. Yang, A. Osinsky, M. A. Khan, and M. S. Shur, IEEE Electron Device Lett. 18, 492 (1997).
- ²²O. Aktas, Z. Fan, S. Mohammad, A. Botchkarev, and H. Morkoc, Appl. Phys. Lett. 69, 3872 (1996).

- ²³S. Arulkumaran, T. Egawa, H. Ishikawa, and T. Jimbo, Appl. Phys. Lett. 80, 2186 (2002).
- ²⁴W. Tan, M. Uren, P. Fry, P. Houston, R. Balmer, and T. Martin, Solid-State Electron. **50**, 511 (2006).
- ²⁵F. Medjdoub, J.-F. Carlin, M. Gonschorek, E. Feltin, M. Py, D. Ducatteau, C. Gaquière, N. Grandjean, and E. Kohn, 2006 International Electron Devices Meeting, San Francisco Hilton and Towers, December 11–13, 2006 (IEEE, Piscataway, NJ, 2006), p. 1.
- ²⁶I. Daumiller, C. Kirchner, M. Kamp, K. J. Ebeling, and E. Kohn, IEEE Electron Device Lett. **20**, 448 (1999).
- 27D. Maier, M. Alomari, N. Grandjean, J.-F. Carlin, M.-A. Diforte-Poisson,
 C. Dua, S. Delage, and E. Kohn, IEEE Electron Device Lett. 33, 985 (2012).
- ²⁸A. E. Islam et al., NAECON 2023-IEEE National Aerospace and Electronics Conference, (IEEE, Piscataway, NJ, 2023), p. 263.
- 29 M. Yuan, Q. Xie, J. Niroula, M. F. Isamotu, N. S. Rajput, N. Chowdhury, and T. Palacios, 2022 IEEE 9th Workshop on Wide Bandgap Power Devices & Applications (WiPDA) (IEEE, Piscataway, NJ, 2022), p. 40.
- ³⁰U. Chowdhury et al., IEEE Electron Device Lett **29**, 1098 (2008).
- ³¹S. Park, C. Floresca, U. Chowdhury, J. L. Jimenez, C. Lee, E. Beam, P. Saunier, T. Balistreri, and M. J. Kim, Microelectron. Reliab. 49, 478 (2009).
- ³²A. E. Islam, N. P. Sepelak, A. T. Miesle, H. Lee, M. Snure, S. Nikodemski, D. E. Walker, N. C. Miller, M. Grupen, K. D. Leedy, K. J. Liddy, A. Crespo, G. R. Hughes, W. Zhu, B. Poling, S. Tetlak, K. D. Chabak and A. J. Green, "Effect of high temperature on the performance of AlGaN/GaN T-gate high-electron mobility transistors with ~140-nm gate length," IEEE Trans. Electron Devices 71(3), 1805–1811 (2024).
- ³³D. Maier et al., IEEE Trans. Device Mater. Reliab. 10, 427 (2010).
- ³⁴Y. Chen, X. Liao, C. Zeng, C. Peng, Y. Liu, R. Li, Y. En, and Y. Huang, Semicond. Sci. Technol. 33, 015019 (2018).
- ³⁵H. Jung, R. Behtash, J. R. Thorpe, K. Riepe, F. Bourgeois, H. Blanck, A. Chuvilin, and U. Kaiser, Phys. Status Solidi C 6, S976 (2009).
- 36 J. Lee, D. Liu, H. Kim, and W. Lu, Solid-State Electron. 48, 1855 (2004).
- 37J. P. Jones, M. R. Rosenberger, W. P. King, R. Vetury, E. Heller, D. Dorsey, and S. Graham, Fourteenth Intersociety Conference on Thermal and Thermomechanical Phenomena in Electronic Systems (ITherm) (IEEE, Piscataway, NJ, 2014), p. 959.
- 38 M. A. J. Rasel, R. Schoell, N. S. Al-Mamun, K. Hattar, C. T. Harris, A. Haque, D. E. Wolfe, F. Ren, and S. J. Pearton, J. Phys. D: Appl. Phys. 56, 305104 (2023). 39 B. Wang, Z. Islam, A. Haque, K. Chabak, M. Snure, E. Heller, and N. Glavin,
- b. Wang, Z. Islam, A. Flaque, K. Chabak, M. Shure, E. Fleher, and N. Glavin Nanotechnology. 29, 31LT01 (2018).
- ⁴⁰Z. Islam, M. Xian, A. Haque, F. Ren, M. Tadjer, N. Glavin, and S. Pearton, IEEE Trans. Electron Devices 67, 3056 (2020).
- ⁴¹Z. Islam, A. Haque, and N. Glavin, Appl. Phys. Lett. 113, 183102 (2018).
- ⁴²L. A. Giannuzzi, B. Kempshall, S. Schwarz, J. Lomness, B. Prenitzer, and F. Stevie, *Introduction to Focused Ion Beams: Instrumentation, Theory, Techniques and Practice* (Springer, New York, NY, 2005), p. 201.
- ⁴³Y. Koyama, T. Hashizume, and H. Hasegawa, Solid-State Electron. 43, 1483 (1999).
- ⁴⁴M. Hÿtch, E. Snoeck, and R. Kilaas, Ultramicroscopy 74, 131 (1998).
- ⁴⁵F. Hüe, M. Hÿtch, H. Bender, F. Houdellier, and A. Claverie, Phys. Rev. Lett. 100, 156602 (2008).
- ⁴⁶W. Gian, M. Skowronski, and G. S. Rohrer, MRS Online Proc. Libr. 423, 475 (1996).
- ⁴⁷M. Hou, S. R. Jain, H. So, T. A. Heuser, X. Xu, A. J. Suria, and D. G. Senesky, J. Appl. Phys. **122**, 195102 (2017).
- ⁴⁸H. Omiya, F. Ponce, H. Marui, S. Tanaka, and T. Mukai, Appl. Phys. Lett. **85**, 6143 (2004).
- 49 Y. Zhou et al., Appl. Phys. Lett. 111, 041901 (2017).
- 50See supplementary material online for discussion on degradation of GaN HEMT due to temperature increase from room temperature to 900°C, incorporating additional information on metal diffusion, layer disappearance, and GPA analysis